Wind Farm Wakes Simulated Using WRF

Pryor, S. C.; Shepherd, T. J.; Barthelmie, Rebecca Jane; Hahmann, Andrea N.; Volker, Patrick

Published in:
Proceedings of the Wake Conference 2019

Link to article, DOI:
10.1088/1742-6596/1256/1/012025

Publication date:
2019

Document Version
Peer reviewed version

Wind Farm Wakes Simulated Using WRF

IOP Conf. Series: Journal of Physics: Conf. Series **1256** (2019) 012025 doi:10.1088/1742-6596/1256/1/012025

Wind farm wakes simulated using WRF

S C Pryor[1], T J Shepherd[1], R J Barthelmie[2], A N Hahmann[3], P Volker[3]

[1] Dept of Earth and Atmospheric Sciences, Cornell University, Ithaca, NY 14853
[2] Sibley School of Mechanical and Aerospace Engineering, Cornell University, Ithaca, NY 14853
[3] Wind Energy Dept, Technical University of Denmark, DK-4000 Roskilde

sp2279@cornell.edu

Abstract. Optimization of wind turbine (WT) arrays to maximize system-wide power production (i.e. minimize 'wind-theft') requires high-fidelity simulations of array-array interactions at the regional scale. This study systematically compares two parameterizations (Fitch and EWP) developed to describe wind farm impacts on atmospheric flow in the Weather Research and Forecasting (WRF) model. We present new year-long simulations for a nested domain centred on Iowa (the state with highest WT density) in the US Midwest that employ real WT characteristics and locations. Simulations with Fitch and EWP indicate similar seasonality in system-wide gross capacity factors (CF) for WT operating in Iowa, but the gross CF are systematically higher in simulations using EWP. The mean gross CF from the Fitch scheme is 44.1%, while that from EWP is 46.4%. These differences in CF are due to marked differences in the intensity and vertical profile of wakes simulated by the two approaches. Output from EWP also indicates much smaller near-surface climate impacts from WT. For example, when summertime hourly near-surface temperature (T2m) from the 299 WT grid cells are compared (i.e. EWP or Fitch minus noWT) the results show warming of nocturnal temperatures (lowest decile of T2m) but the maximum warming is considerably larger in simulations with the Fitch scheme.

1. Introduction

Wind turbine (WT) deployments in the USA have shown strong growth over the last few years and remain dominated by the onshore market (Fig. 1) [1]. A recent report by the U.S. Federal Energy Regulatory Commission concluded that proposed generation and retirements by December 2021 include net capacity additions by renewable sources of 169,914 MW. That is 4.3 times greater than the net new additions listed for coal, oil, and natural gas combined (39,414 MW). Net proposed additions from wind alone total 90,268 MW [2].

A decrease in the mean wind speed (U) and enhancement of the turbulent kinetic energy (TKE) downstream from WT arrays is inevitable. Optimizing expansion of the number of WT to maximize power production (i.e. minimize 'wind-theft') and/or allowing potential wind farm developers to make informed decisions regarding optimal sites for development requires high-fidelity simulations of array-array interactions at the regional scale. The projected expansion of the WT fleet and installed capacity may also have implications for local/regional climates in the deployment locations that can also only be assessed *a priori* using high resolution numerical simulations [3]. Addressing these questions and evaluating tools available for regional scale simulations of array effects are the motivations for the research reported herein.

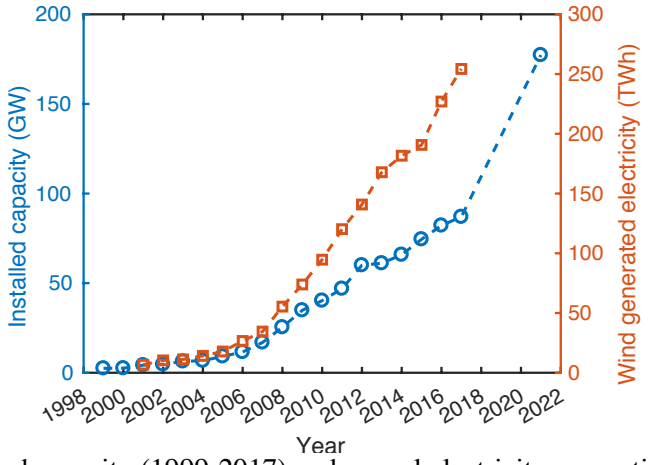

Figure 1. Installed wind capacity (1999-2017) and annual electricity generation in the USA (2001-2017), and the projected installed capacity in 2021. Data regarding installed capacity downloaded from: https://windexchange.energy.gov/maps-data/321, data on annual electricity generation downloaded from https://www.eia.gov/renewable/data.php.

2. Methods

2.1 Wind farm parameterizations in WRF

This study systematically compares two wind farm parameterizations in terms of:

(1) Wake profiles simulated near and downwind of wind turbine arrays and system-wide power production efficiency as measured by gross capacity factors (CF).

(2) Effects of WT arrays on near-surface air temperature and specific humidity.

Both wind farm parameterizations were designed for use in the Weather Research and Forecasting (WRF) model and explicitly exclude treatment of near-wake dynamics, but instead seek to describe the ensemble far wake from all WT within a WRF grid cell. They simulate the net effect on flow and depict the change in spatially average properties (denoted in Table 1 using <>). Both are designed for use with geolocated WT and their hub height (HH), rotor diameter (D), power and thrust curves. The WT are parameterized such that each applies a (local) drag force to act as a momentum sink to all model grid cells that intersect the turbine rotor. The drag applied and TKE introduced is determined by the incident wind speed and WT specifications. Main features of the parametrizations are summarized in Table 1.

Table 1. Synthesis of the two wind farm parameterizations compared herein.
Note: dU = change in wind speed induced by the action of WT(s).

Property	**Fitch** [4,5]	**Explicit Wake Parameterization (EWP)** [6]
<Thrust (drag) force>	Applied to vertical grid cells in the rotor plane (proportional to <dU>)	Applied to vertical grid cells in the rotor plane (proportional to <dU>) Within grid cell wake expansion treated using diffusion equation & effective thrust force
<TKE>	Shear production + WT ($f(U^3)$)	Shear production only
<U> in neutral conditions	Max dU above HH Speed-up at lowest layer	Max dU at HH

2.2 Simulations

Previous research has suggested that inadvertent flow and climate modification from WT arrays exhibits a substantial dependence on the wind farm parameterization used in WRF [7]. Here we present new simulations conducted using WRF (v3.8.1) for the nested domain shown in Fig. 2. A key advance in the current research relative to our earlier work which employed two sets of independent paired simulations

is that there is a single outer domain and multiple inner domains. The outer domain (d01) is resolved at 12 km and comprises 149 × 149 grid cells. Three inner domains are nested within d01, are simultaneously computed, cover the same area and all three are discretized 4 km. The three inner domains differ only with respect to the wind farm parameterization:

- d02-noWT: no WT parameterization is employed
- d02-Fitch: Uses georeferenced WT locations and specifications and employs the Fitch parameterization to describe the wind farm effects. Two-hundred and ninety-nine of the grid cells within d02 contain one or more operating WT as of the end of 2014 (WT records obtained from: https://eerscmap.usgs.gov/arcgis/rest/services/wind/wTurbinesWMDyn/MapServer).
- d02-EWP: WT specifications as in d02-Fitch but uses the EWP wind farm parameterization.

Lateral boundary conditions are supplied every 6-hours from the ERA-Interim reanalysis data [8]. The NOAA Real Time Global Sea Surface Temperature (RTG-SST) data provides initial SST and Great Lakes conditions and are updated every 24 hours. The simulations were conducted for November 2007 to November 2008, inclusive with the first month used as spin up, thus results presented herein are for December 2007 to November 2008, inclusive.

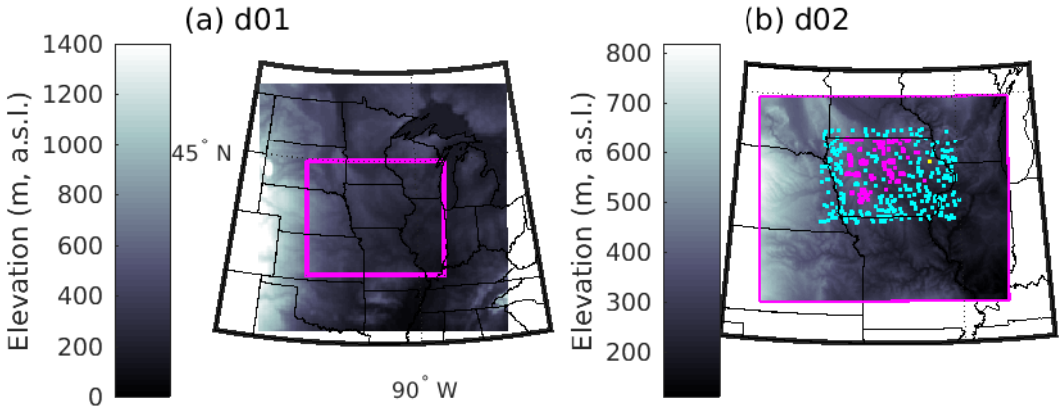

Figure 2. (a) Outer domain (d01) with the mean elevation in each 12 km × 12 km grid cell. The magenta outline shows the area covered by the inner domains. (b) Inner domains (d02-noWT, d02-Fitch, d02-EWP) and the mean elevation in each 4 km × 4 km grid cell. Grid cells that contain WT are shown in magenta and the no-WT (background) grid cells used for comparative analyses shown in cyan. The Elk wind farm in eastern Iowa is denoted by the yellow symbols. This wind farm comprises 17, 2.5 MW wind turbines (HH = 100 m) and is contained within two grid cells.

In all domains there are 41 vertical levels up to a model top of 50 hPa, 18 of these levels are in the lowest 1 km of the atmosphere. The following physics schemes are applied: Longwave radiation: Rapid radiative transfer model (RRTM) [9]. Shortwave radiation: Dudhia [10]. Microphysics: Eta (Ferrier) [11]. Surface-layer physics: MM5 similarity scheme [12]. Land surface physics: Noah land surface model [13]. Planetary boundary layer: Mellor-Yamada-Nakanishi-Niino 2.5 [14]. Cumulus parameterization: Kain-Fritsch [15] is used in d01 while d02-noWT, d02-Fitch and d02-EWP are sufficiently highly resolved (4 km) that no cumulus scheme is applied.
Three-dimensional fields of the wind components and power output are output every 10-minutes, while near-surface air temperature and specific humidity are output once hourly.

3. Results

3.1 Power production and capacity factors

Gross capacity factors (CF) are computed as the ratio the sum of electrical power produced by each scheme in each 10-minute period to the maximum possible as determined by the cumulative nameplate capacity for all WT in Iowa. These gross CF exceed net CF from operating wind farms [16] because gross CF exclude factors such as curtailment, downtime for maintenance and also near-wake effects since all WT within a grid cell experience the same inflow wind speed. Nevertheless, they permit

comparative analyses of the two schemes. Simulations with the Fitch and EWP wind farm schemes indicate similar seasonality in system-wide gross CF. In d02-Fitch the median 10-minute gross CF in each month range from 25% in July to a high of > 55% in April (Fig. 3). However, gross CF are systematically higher in power output from the EWP domain (d02-EWP) (Fig. 4). The mean (median) gross CF derived using power production data for all 12 months and all WT in Iowa from d02-Fitch is 44.1% (39.6%), while that from d02-EWP is 46.4% (43.5%). The interquartile range of all 10-minute system-wide gross CF is; 15.6 to 71.2% for d02-Fitch and 17.9 to 74.5% for d02-EWP.

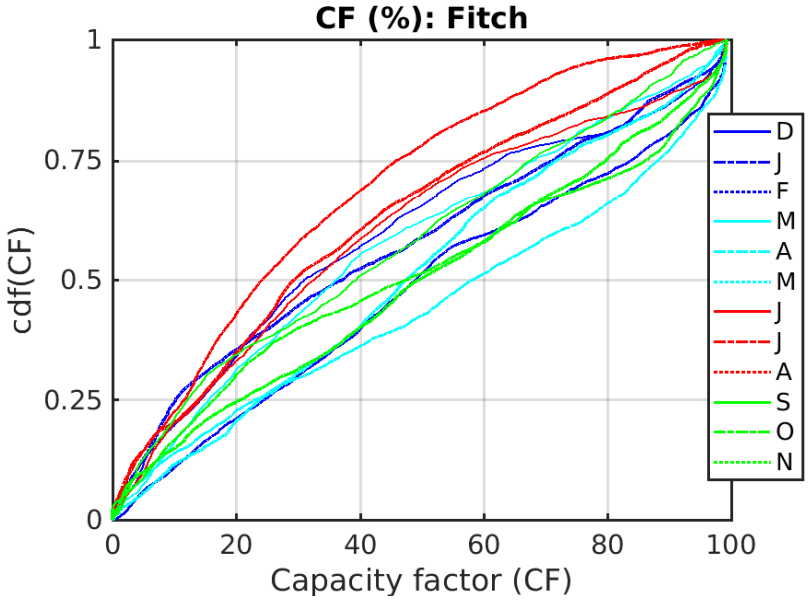

Figure 3. Cumulative density function (cdf) for 10-minute gross capacity factors (CF, shown in %) based on power output from all WT in Iowa for each calendar month (December 2007 to November 2008) computed for the domain using the Fitch wind farm parameterization (d02-Fitch).

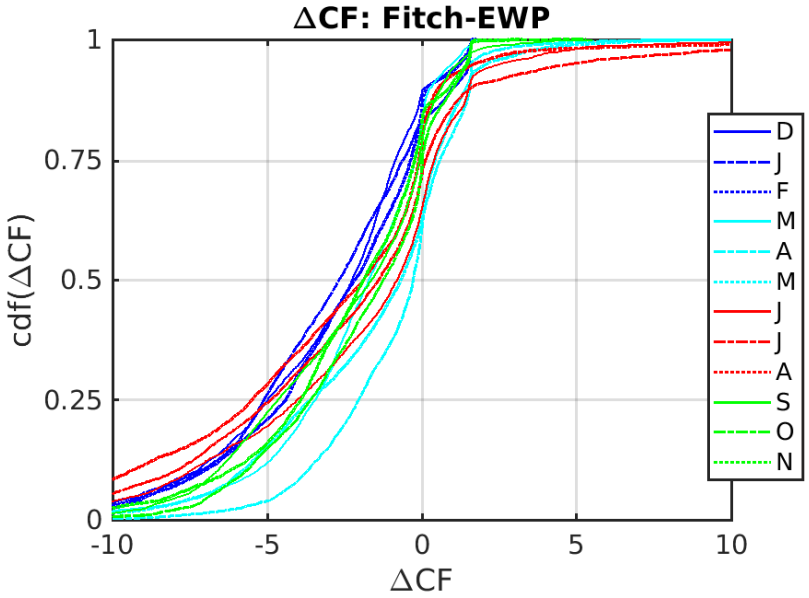

Figure 4. Cumulative density function (cdf) for differences in pairwise 10-minute gross capacity factors (ΔCF, i.e. CF in % from Fitch minus the value from EWP) based on power output from all WT in Iowa for each calendar month (December 2007 to November 2008). ΔCF is computed using 10-minute power output from d02-Fitch minus d02-EWP.

In all months, 60 to 90% of 10-minute periods exhibit higher gross CF when the EWP scheme is adopted than when the Fitch parameterization is used (Fig. 4, Table 2). This implies that system-wide total power production from WT in Iowa is higher for a substantial fraction of 10-minute periods in simulations that use the EWP parameterization. For example, in May 2008 61% of 10-minute periods have higher CF for simulations with EWP than Fitch, while in December 2007 83% of 10-minute periods exhibited higher CF in d02-EWP than in d02-Fitch.

Table 2. Percentile at which the difference in gross CF (computed pairwise from 10-minute power production from Fitch and EWP as the CF from Fitch minus the CF from EWP, i.e. d02-Fitch – d02-EWP) is equal to zero by month from December 2007 (D) to November 2008 (N).

	D	J	F	M	A	M	J	J	A	S	O	N
Percentile	83	89	83	85	83	61	63	65	72	79	79	73

Higher system-wide gross CF are observed when the EWP scheme is applied because it generates smaller velocity deficits within grid cells containing WT. Thus, less intense wakes are advected downstream from those grid cells. Additionally, this formulation projects slightly more rapid recovery of wakes from upstream arrays. An illustrative example of the differences in wake profiles is given in Fig. 5 for the Elk wind farm (see location in Fig. 2). These composite profiles reflect data from all cases of northerly flow (i.e. a wind direction of 355° to 5°) in the upstream grid cell at WT HH during July 2008 when the wind farm was generating 25-30 MW (cf. total nameplate capacity of 42.5 MW). The velocity deficit recovers to the freestream (i.e. the velocity deficit throughout the vertical profile relative to d02-noWT is almost zero) at approximately seven 4 km grid cells downstream (~ 24-28 km from the edge of the grid cells containing the wind farm). As shown, the vertical wake profiles both within and downstream of the wind farm are markedly different in simulations with EWP and Fitch.

Consistent with differences in the formulation of the two schemes, the height of maximum velocity deficit is displaced upward from the WT HH in Fitch, but is centered on the HH in simulations with EWP. Use of the Fitch scheme also causes increased (area-averaged) wind speeds at the lowest model level in grid cells where WT are deployed. The maximum velocity deficit as simulated using the Fitch scheme is of larger magnitude than that generated by the EWP scheme in all grid cells. The difference in the velocity deficit within WT grid cells may be due to the explicit inclusion in the EWP scheme of within grid cell wake expansion (Table 1). The premise behind treatment of this effect is that there is expansion of the volume of air affected by the wake directly downstream of WT and that effect is not negligible within one WRF grid cell for any reasonable resolution at which WRF is applied. Further, this effect is dominated by expansion in the vertical direction. This part of the wake expansion is not accounted for in the mesoscale model, and so is described using a sub-grid-scale diffusion equation to generate an effective thrust force which is applied within the Reynolds Averaged Navier-Stokes (RANS) equations within the WRF model (see details in [6]). The wake profile as applied in EWP to account for the within grid expansion is dependent on a length scale that was calibrated using observations from an offshore wind farm [6]. The TKE added in the Fitch scheme due to the 'unresolved' action of the WT on the atmosphere plays a similar role in enhancing wake expansion but is not realized within the grid cell and is defined as the power extracted by the WT but not converted into electrical power.

Differences between the two wind farms schemes was previously noted in an application to an 80 WT offshore wind farm where WRF was applied at a horizontal resolution of ~ 1 km [6]. That analysis found faster initial wind farm wake recovery for simulations with the Fitch scheme (referred to therein as WRF-WF). The authors reported that 'The 10 % velocity deficit contour, for example, extends for the EWP scheme to around x = 15 km, while for the WRF-WF scheme it extends to x = 8 km. The difference in the distance at which a 7.5 % velocity deficit is reached is even larger: after x = 21 and x = 11 km for the EWP and WRF-WF scheme, respectively. Further downstream, after around 30 km, the velocity fields from the two parametrizations become similar' [6]. It appears that in that offshore case the addition of larger amounts of TKE in the Fitch scheme dominates the differences in wake behavior and may have resulted in faster wake recovery due in part to the lower ambient turbulence offshore. The converse is likely observed here because higher ambient turbulence (and vertical shear) over land areas reduces the

importance of the additional TKE from the Fitch scheme and thus the differences between the schemes are more dominated by within grid cell diffusion of the wake in EWP.

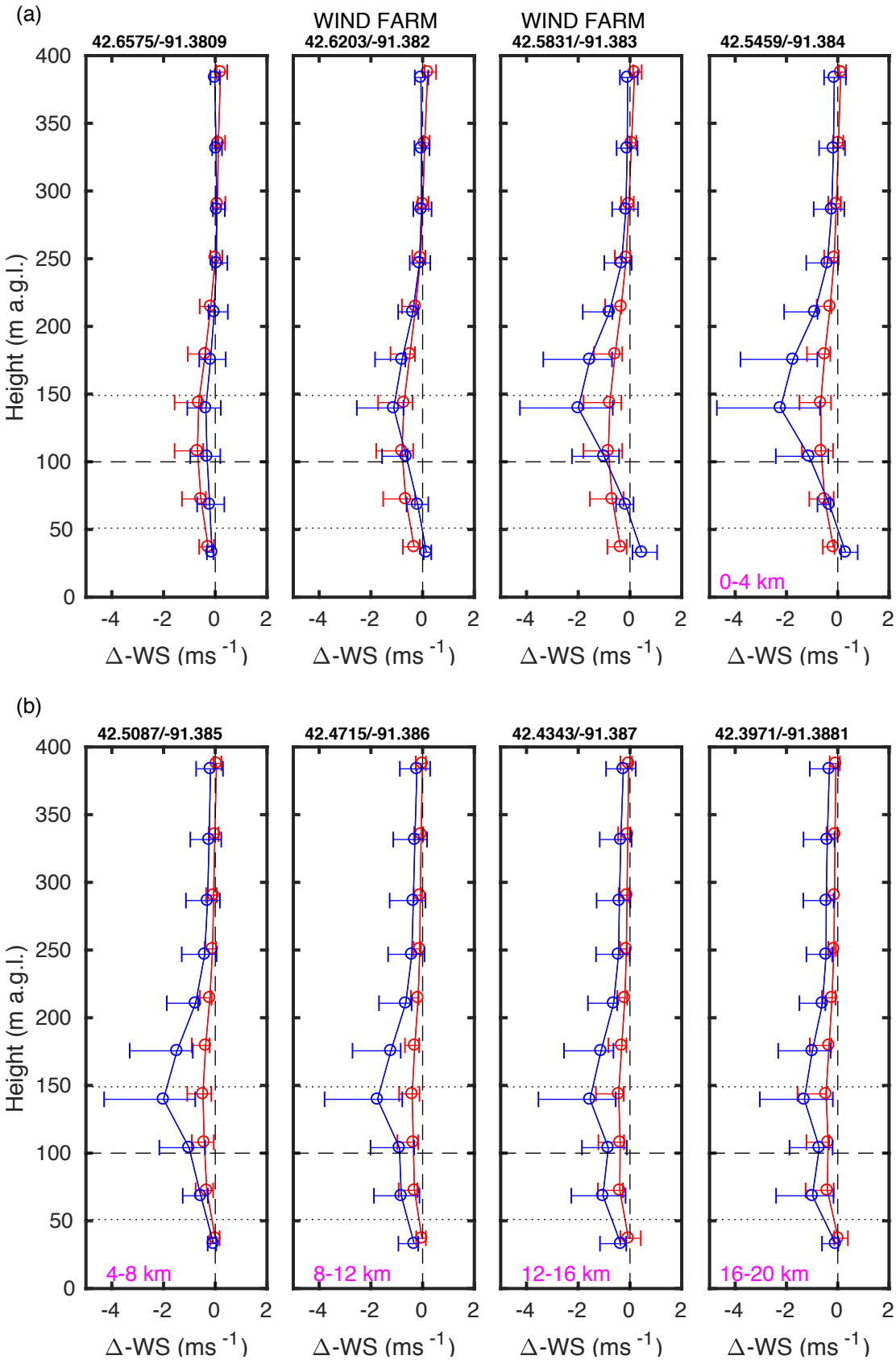

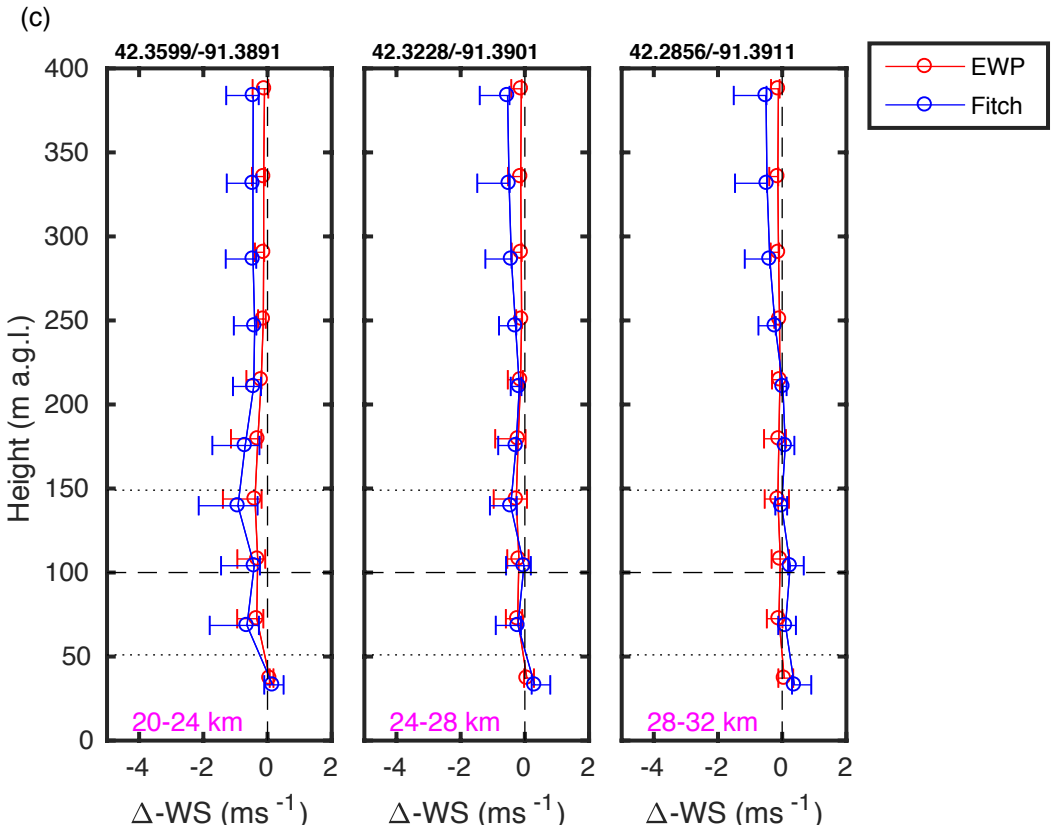

Figure 5. Mean velocity deficits (Δ-WS) computed as the pairwise difference; output from d02-Fitch or d02-EWP minus that from d02- noWT for northerly flow. The panels show Δ-WS upstream of the Elk wind farm (first panel in (a)), over the wind farm (central panels of (a)) and for increasing downstream distances (last panel of (a), and panels in (b) and (c)). Downstream distances from the wind farm are indicated by the numbers shown in magenta in the lower left of each panel. The grid cell centroid latitude (N) and longitude (E) are shown in the title of each panel. The mean velocity deficit is shown by the symbol, the horizontal error bars show the minimum and maximum velocity deficits for any 10-minute period at each model height for each scheme (Fitch or EWP). Horizontal dashed lines in each panel show the HH (100 m) and the upper and lower tip of the rotor plane.

3.2 Near-surface climate impacts

Previous research has indicated largest perturbation of near-surface climate over Iowa are derived using WRF simulations with the Fitch scheme during the summer months [3]. Thus, hourly output of near-surface (2-m) air temperature (T2m) and specific humidity (Q2m) were compared from the inner domains; d02-noWT, d02-Fitch and d02-EWP for the 299 grid cells with WT present and 299 background grid cells located at least six grid cells from the closest WT (locations shown in Fig. 2). For each grid cell the probability distribution for the 1st to 99th percentile of T2m (or Q2m) is computed for d02-noWT, d02-Fitch and d02-EWP. Differences in those percentile values (e.g. d02-Fitch minus d02-noWT, ΔT) for that grid cell are also computed. Then the mean difference, maximum positive and maximum negative difference at each percentile of the T2m distribution are computed for all 299 WT grid cells. A comparable analysis is done for the 299 background grid cells. If, at a given percentile of the T2m distribution, the mean difference is close to zero and the maximum positive and maximum negative deviations are symmetric around zero, it implies that the action of WT in a grid cell is equally likely to generate warm or cold anomalies, and that there is no systematic influence from WT on that percentile of near-surface air temperatures. As shown by Fig. 6, both the EWP and Fitch schemes indicate WT tend to warm the coolest hours (i.e. lowest percentiles of summertime T2m) in the grid cells where they are located. The 5th percentile T2m for the 299 WT grid cells has a mean value of 12.3°C. The warming due to WT is approximately 1.1°C for the 5th percentile T2m when using the Fitch

scheme, and approximately 0.3°C for EWP. Thus, according to this simulation, for the coldest 5% of hours, the action of WT in generating enhanced mixing tends to result in warming the near-surface air temperatures of between 0.3 and 1.1°C. This perturbation of T2m is larger and more positive in Fitch than EWP for all percentiles of the T2m distribution. The difference in T2m in grid cells with WT greatly exceeds that for the background grid cells, which is zero for both Fitch and EWP for all percentiles. This indicates that the non-local effect on near-surface temperature is virtually zero, but consistent with experimental research (Table 3), night-time T2m near WT are elevated relative to background locations. The mean impact of WT on near-surface air temperature decreases as the percentile under consideration increases as does the maximum perturbation in any WT grid cell (Fig. 6). This is also consistent with experimental research that shows little impact from WT on daytime T2m (Table 3).

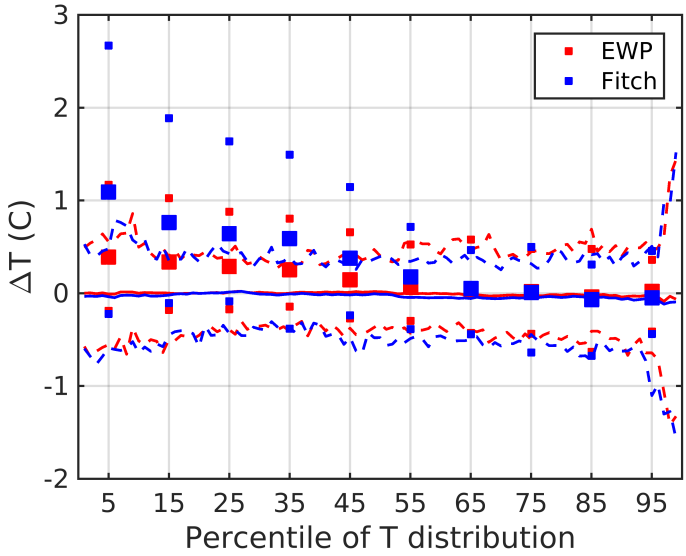

Figure 6. The maximum positive, mean and maximum negative difference in hourly near-surface air temperature (ΔT) from d02-Fitch or d02-EWP versus d02-noWT as a function of the percentile of the T2m distribution in d02-noWT. Solid symbols show the mean (largest symbol) and largest positive and negative anomalies (smaller symbols) in any WT grid cell at that percentile (in 5% increments). The lines show the same but for the background (noWT) grid cells (shown for 1st-99th percentile). Red depicts results for d02-EWP relative to d02-noWT, while blue shows d02-Fitch relative to d02-noWT.

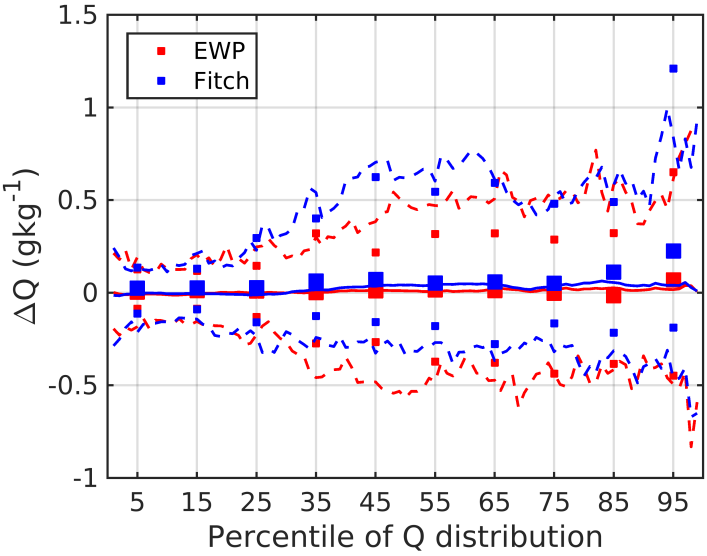

Figure 7. As Fig. 6 but for hourly near-surface specific humidity (ΔQ) from d02-Fitch or d02-EWP versus d02-noWT as a function of the percentile of the Q2m distribution in d02-noWT.

The effect on near-surface specific humidity is more complex in part because of the key role of soil moisture in determining the latent heat flux (and limitations thereon) and thus Q2m. The mean impact from WT on summertime Q2m in grid cells containing WT is close to zero except during the most humid hours (95th percentile) when the presence of WT appears to increase Q2m with, again, a larger magnitude effect in when the Fitch parameterization is employed (Fig. 7).

Table 3. Example experimental research in the US Midwest on WT impacts on local near-surface temperature.

Ref.	Approach	Study area	Season	Summary of results
[17]	In situ measurements	> 200 WT in flat terrain (HH = 80 m). Indiana	Apr & May	At 2.1 km downstream: Inc. nighttime T2m ≤ 1.6°C. Dec. daytime T2m ≤ 0.24°C (not statistically sign.)
[18]	In situ measurements	Two rows of 13 WT in Iowa	Late Jun to early Sep	No difference in daytime T2m. Warming of night-time T2m (0.4°C).
[19]	Difference in seasonal mean nighttime (10:30pm) land surface temperature (LST) from MODIS satellite obs.	Five wind farms in Iowa	All	Differences: WT pixels MINUS non-WT Spring: -0.093 to 0.365°C Summer: 0.119 to 0.259°C Fall: 0.181 to 0.485°C No signal in winter

4. Concluding remarks

No definitive statement can yet be made about which wind farm parameterization (Fitch or EWP) scheme is more accurate. However, the CF differences reported herein are of sufficient magnitude to impact wind farm economics and efforts to optimize multiple array developments. The mean CF derived using all 10 minute power production data for WT in Iowa from the Fitch scheme is 44.1%, while that from EWP is 46.4%. These differences in system-wide power production reflect important differences in the intensity of wind farm wakes from the two schemes. These results may have important implications for the US wind energy industry given the rapid expansion of installed capacity and that a substantial fraction of the new capacity may be added in the potential wind-shadow of existing arrays.

Consistent with the less intense and persistent downstream wakes in the EWP scheme, local climate impacts are also more pronounced when the Fitch scheme is applied. For example, mean estimated perturbations in T2m in WT grid cells during the coldest 5% of summertime hours are up to +1.1°C in d02-Fitch but only +0.3°C when the EWP parameterization is applied.

The Fitch scheme has been more widely used in previous analyses of array-array interactions and local climate perturbations. Thus, results presented herein suggest the literature (see review in [3]) may systematically overstate wake effects and climate impacts from WT arrays deployed onshore. Advanced large-scale experiments of the far wake conditions downstream of large operating onshore wind farms are needed to generate the empirical data necessary to evaluate the skill of the two wind farm parameterizations.

5. References

[1] AWEA. AWEA: 3rd Quarter 2018 Market Report. 42 (Available for purchase from http://www.awea.org/, 2018).

[2] Froese, M. FERC data suggests renewable capacity could be quadruple that of fossil fuels by 2021. *Windpower Engineering and Development*, https://www.windpowerengineering.com/business-news-projects/research-reports/ferc-data-

suggests-renewable-capacity-could-be-quadruple-that-of-fossil-fuels-by-2021/ (2019).
[3] Pryor, S. C., Barthelmie, R. J. & Shepherd, T. 2018. The influence of real-world wind turbine deployments on regional climate. *J. Geophys. Res.-Atmos.* **123**, 5804-5826 (doi: 5810.1029/2017JD028114).
[4] Fitch, A. C. *et al*. 2012. Local and Mesoscale Impacts of Wind Farms as Parameterized in a Mesoscale NWP Model. *Monthly Weather Review* **140**, 3017-3038, doi:10.1175/mwr-d-11-00352.1.
[5] Fitch, A. C. 2016. Notes on using the mesoscale wind farm parameterization of Fitch et al.(2012) in WRF. *Wind Energy* **19**, 1757-1758.
[6] Volker, P. J. H., Badger, J., Hahmann, A. N. & Ott, S. 2015. The Explicit Wake Parametrisation V1.0: a wind farm parametrisation in the mesoscale model WRF. *Geoscientific Model Development* **8**, 3481-3522. doi:3410.5194/gmdd-3488-3481-2015.
[7] Pryor, S. C., Barthelmie, R. J., Hahmann, A. N., Shepherd, T. J. & Volker, P. J. H. 2018. Downstream effects from contemporary wind turbine deployments. *Journal of Physics: Conference Series* **1037**, doi :10.1088/1742-6596/1037/1087/072010.
[8] Dee, D. P. *et al*. 2011. The ERA-Interim reanalysis: Configuration and performance of the data assimilation system. *Quarterly Journal of the Royal Meteorological Society* **137**, 553-597.
[9] Mlawer, E. J., Taubman, S. J., Brown, P. D., Iacono, M. J. & Clough, S. A. 1997. Radiative transfer for inhomogeneous atmospheres: RRTM, a validated correlated-k model for the longwave. *Journal of Geophysical Research: Atmospheres* **102**, 16663-16682.
[10] Dudhia, J. 1989. Numerical study of convection observed during the winter monsoon experiment using a mesoscale two-dimensional model. *Journal of the Atmospheric Sciences* **46**, 3077-3107.
[11] Ferrier, B. S. *et al*. 2002. Implementation of a new grid-scale cloud and precipitation scheme in the NCEP Eta model. *15th Conf. on Numerical Weather Prediction*, 280-283.
[12] Beljaars, A. 1995. The parametrization of surface fluxes in large-scale models under free convection. *Quarterly Journal of the Royal Meteorological Society* **121**, 255-270.
[13] Tewari, M. *et al*. 2004. Implementation and verification of the unified NOAH land surface model in the WRF model. *20th Conference on Weather Analysis and Forecasting/16th Conference on Numerical Weather Prediction* **1115**, 6pp.
[14] Nakanishi, M. & Niino, H. 2006. An improved Mellor–Yamada level-3 model: Its numerical stability and application to a regional prediction of advection fog. *Boundary-Layer Meteorology* **119**, 397-407.
[15] Kain, J. S. 2004. The Kain–Fritsch convective parameterization: an update. *Journal of Applied Meteorology* **43**, 170-181.
[16] Pryor, S. C., Shepherd, T. J. & Barthelmie, R. J. 2018. Interannual variability of wind climates and wind turbine annual energy production. *Wind Energy Science* **3**, 651-665.
[17] Smith, C. M., Barthelmie, R. J. & Pryor, S. C. 2013. In situ observations of the influence of a large onshore wind farm on near-surface temperature, turbulence intensity and wind speed profiles *Environmental Research Letters* **8**, 034006.
[18] Rajewski, D. A., Takle, E. S., Prueger, J. H. & Doorenbos, R. K. 2016. Toward understanding the physical link between turbines and microclimate impacts from in situ measurements in a large wind farm. *Journal of Geophysical Research: Atmospheres* **121**, 13392-13414.
[19] Harris, R. A., Zhou, L. & Xia, G. 2014. Satellite observations of wind farm impacts on nocturnal land surface temperature in Iowa. *Remote Sensing* **6**, 12234-12246.

Acknowledgments
This work was support by the U.S. Department of Energy (DoE) (DE-SC0016438), Cornell University's Atkinson Center for a Sustainable Future (ACSF-sp2279-2016). The research used computing resources from the National Science Foundation (ACI-1541215) and the NSF Extreme Science and Engineering Discovery Environment (XSEDE) (allocation award to SCP is TG-ATM170024) and computing resources from DoE (DE-AC02-05CH11231).